Egyptian Geophysical Society
EGS Journal, Vol. 21, No. 1, 1-10 (2023)

BUILDING OF STRUCTURAL MODEL AND FAULT SEAL ANALYSIS AT FERDAUS OIL FIELD, SOUTHEAST ABU GHARADIG BASIN, WESTERN DESERT, EGYPT

R. ISMAIL[(1)], A. EL-WERR[(2)] and A. HELALY[(2)]

(1) North Bahariya Petroleum Company
(2) Geophysics Department, Faculty of Science, Ain Shams University

بناء نموذج تركيبى وتحليل الصدوع المسدودة في حقل فردوس للبترول، جنوب شرق حوض أبو الغراديق، الصحراء الغربية ، مصر

الخلاصة: تشمل نمذجة الخزان الهيدروكربونى نوعين رئيسيين: النمذجة الجيولوجية (النموذج الإستاتيكى) ونمذجة المحاكاة (النموذج الديناميكي). وتتمثل أهداف نمذجة الخزان تخليق تقييم دقيق للأحجام الكلية والصافية للخزان، وإحتياطى البترول الموجود (OOIP) – حيث أنها مهمة جدا في تقييم اقتصاديات خطة تطوير الخزان. يتم إنشاء النموذج الإستاتيكى بواسطة الجيولوجيين والجيوفيزيائيين لتقديم وصف إستاتيكى للخزان قبل الإنتاج بينما يتم إنشاء النموذج الديناميكي من قبل مهندسي الخزان لمحاكاة تدفق الموائع داخل الخزان على مدار عمر الإنتاج. في هذا العمل الحالي ، تعطي نتائج التفسير السيزمى التركيب الجيولوجى لحقل فردوس للبترول وهو عبارة عن كتلة شديدة الميول مصدوعة فى إتجاه شمال غرب–جنوب شرق. وتأخذ معظم الصدوع الرئيسية إتجاه شمال غرب–جنوب شرق و شرق–غرب و شمال–جنوب. ويتطلب بناء النموذج التركيبى النهائى ثلاثى الأبعاد الخطوات التالية: عمليات نمذجة الصدع، وشبكات الأعمدة، وعمل أسطح طبقات وعمل نطاقات لتأكيد التراكيب المفسرة من البيانات السيزمية. تم اختبار خمسة آبار محفورة في حقل فردوس للبترول وتحديد الوضع الإقليمي لهذا الجزء من الصحراء الغربية. وتشكل أهداف الخزان الرئيسية في أبو رواش "G" الأوسط والسفلي وتكوين البحرية العليا كتل صدعية مائلة لقفلة مائلة فى ثلاثة إتجاهات. ويظهر الصدع المسدود من تقابل صخور الخزان / مع صخور الغير الخزان. وتم استخدام طريقة الرسم البيانى للعالم ألان لتحديد الخزانات المتقابلة لتقييم جهد تدفق الموائع عبر مضرب الصدع ورسم خريطة لمستوى الصدع مع تقاطعات الحائط العلوى والحائط السفلى على سطح الصدع. ويقابل خزانات أبو رواش "G" الأوسط والسفلى والبحرية العليا في الحائط السفلى فى الجانب العلوى جنبا إلى جنب مع أعضاء طمي وطفلة أبو رواش "E"، والحجر الجيري لأبو رواش "F" وصخور طفلة السد لأبو رواش "G" العلوي في الحائط العلوى للجانب السفلى (سد داخل التكوين)..

ABSTRACT: *Reservoir modeling typically falls into two main categories: geological modeling (static model) and reservoir simulation modeling (dynamic model). The objectives of the integrated reservoir modeling are to create a reliable evaluation of the bulk and net reservoir volumes, and the original hydrocarbons in place - which are of utmost importance in assessing the economics of a reservoir development project. Static model is created by geophysicists and geologists to provide a static description of the reservoir, prior to production whereas dynamic model is created by reservoir engineers to simulate the flow of fluids within the reservoir, over its production lifetime.*

In the present study, seismic interpretation yields Ferdaus oil field structure which is a northwest-southeast oriented highly faulted tilted block. Most faults are trending northwest-southeast or east-west, while a few trend north-south.

Fault modeling, pillar gridding, make horizons and make zones processes were created and added together to build the final 3D structural model. The obtained final 3D structural model confirms the interpreted structure yielded from the seismic interpretation.

The five wells drilled in the Ferdaus oil field tested and identified the regional setting of this part of the Western Desert by having northwest-southeast structure trend at Middle and Lower Abu Roash "G" and Bahariya Formation target levels as a big horst block which is divided into smaller three-way dip closure tilted fault blocks by different fault trends.

Fault seal can arise from reservoir/non-reservoir juxtaposition. Allan diagram method was used to determine the juxtaposed reservoirs for evaluating the flow potential across a fault strike and mapping the fault plane with the hanging wall and footwall intersections superimposed on the modeled fault surface.

The Middle Abu Roash "G", Lower Abu Roash "G" and Upper Bahariya reservoirs in the footwall upthrown are juxtaposed by Abu Roash "E" silt and shale, Abu Roash "F" Limestone and Upper Abu Roash "G" shale seal Members in the hanging wall downthrown side.

INTRODUCTION

The North Bahariya Concession lies on the southeastern part of the Abu Gharadig Basin which is one of the main petroleum producing basins in the Western Desert about 150 km west of Cairo as shown in the study area location map (Fig. 1). The concession was first explored by Amoco, from the late 60's until the early 90's. The area was then awarded to IPR in April 1998 for an initial exploration period of three years. The first exploration success came with the drilling of well NB-1X in May 2000, on a structure previously drilled

by Amoco (well WQ56/4-1, drilled in 1990). The modest results of the NB-1X well did not justify a stand-alone development.

The Ferdaus Oil Field (Fig. 2) is contained within the stratigraphic sequence of Abu Gharadig Basin. Ferdaus oil field is mainly producing from the Upper Cretaceous (Cenomanian): Upper Bahariya, Middle and Lower Abu Roash G (ARG) sandstones, as shown in **(Fig. 3)**. These reservoirs were deposited in a fluvial to shallow marine environment exposed to tidal influence and eustatic fluctuations in sea level. The Upper Bahariya represents a shoreline depositional environment, characteristics of barrier bar and for the channel sands. The environment of deposition for ARG reservoir sands was a wide long-shore tidal ridge, resulting in the deposition of sand bars and beach ridges. These bars and ridges can be connected, resembling a sheet-like sand deposit.

Methodology

1) Seismic Interpretation

The geologic horizons were picked along all of the available seismic sections using computer program (Petrel 2014) software developed by Schlumberger Service Company and tying loops using intersection points of these lines and composite wells passing through them. These seismic reflection horizons are arranged from young to old and representing the following geologic formation tops: Top Middle and Lower Abu Roash G members and Upper Bahariya Formation reservoir targets.

Fig. 4 shows a 2D seismic line 5462 in the dip direction (S-N) passing through Ferdaus-1 and Ferdaus-12 wells that are used for geological formation tops identification and correlation during a well-to-seismic tie. This seismic line shows three normal faults (F1, F2 and F3) in the central part dissecting the interested formation tops. F1 and F2 normal faults are downthrown to the SW with different throws and heaves, while F3 normal fault is downthrown to the NE.

Ferdaus-12 well was drilled to explore Middle and Lower Abu Roash "G" reservoir sands as a primary targets in a separate three-way dip closure block (Fig. 5)

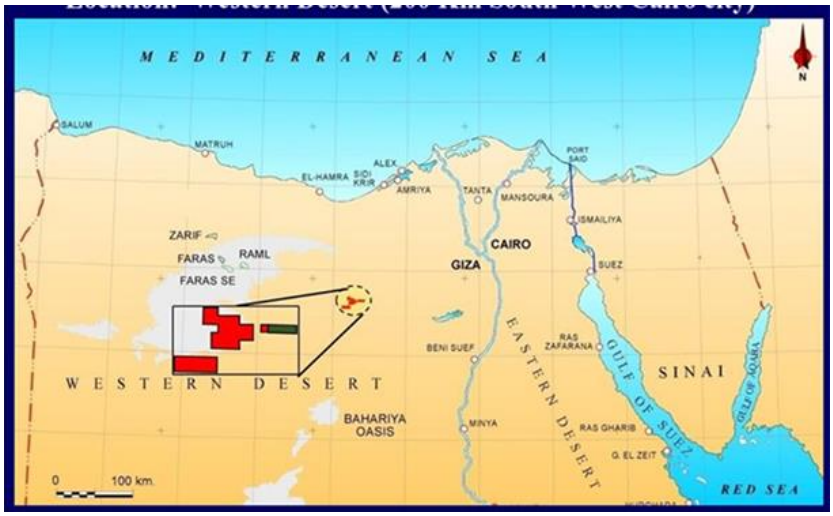

Fig. (1): Location map of the North Bahariya Concession.

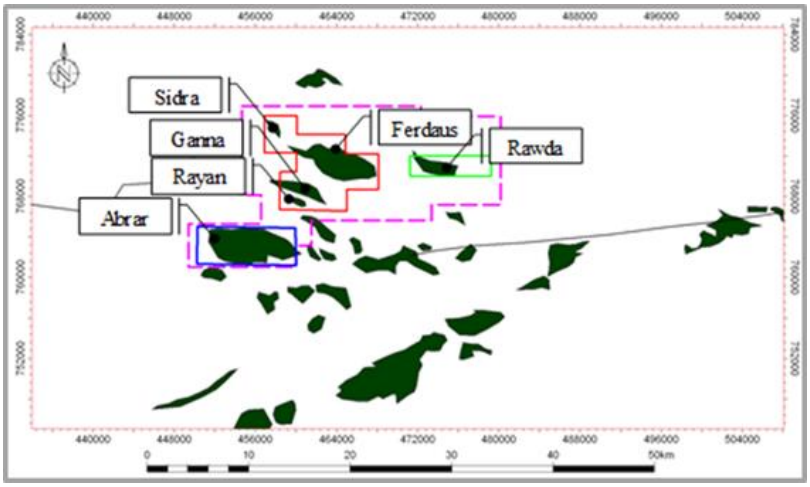

Fig. (2): Ferdaus Oil Field location map.

along the main up-thrown side block of the Ferdaus-1 well E-W/WNW-ESE trending play fault (F2). The Middle and Lower Abu Roash "G" sands are completely missed in the Ferdaus-1 well.

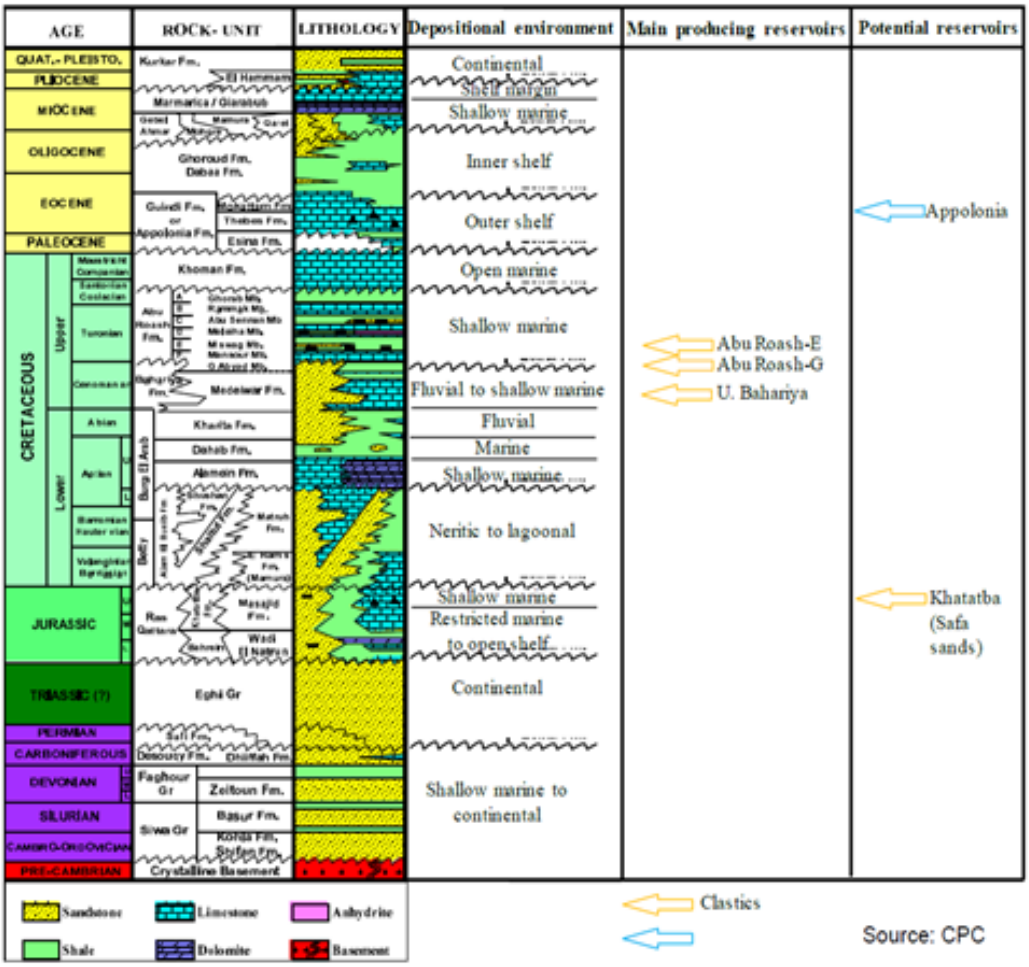

Fig. (3): Abu Gharadig basin stratigraphic column (after Abdel Aal and Moustafa, 1988).

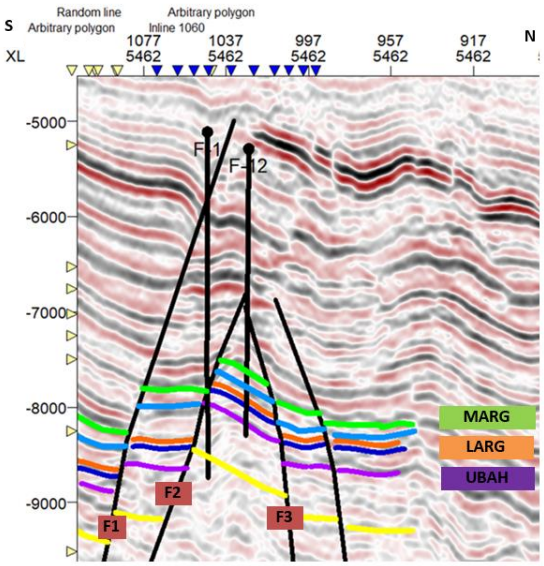

Fig. (4): Interpreted S-N seismic line 5462 passing by Ferdaus-1 and Ferdaus-12 wells.

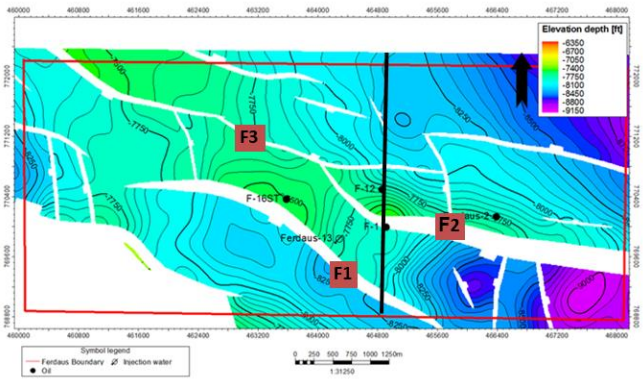

Fig. (5): Depth structure map on the top of Middle Abu Roash G.

2) Reservoir Modeling

The main types of reservoir modeling are typically the static modeling and dynamic modeling. Construction of the reservoir model benefited from many discussions of the reservoir team: geologic modeler, geologists, petrophyscist, geophysicist and reservoir engineer. The goal was to construct a reservoir model that was adequately representative of the heterogeneities seen within the reservoir, detailed in its description, yet allowed easy modification of individual parameters through its evolution (Abdul Azim et al., 2003).

Static model is created by geophysicists and geologists to provide a static description of the reservoir, prior to production whereas dynamic model is created by reservoir engineers to simulate the flow of fluids within the reservoir, over its production lifetime.

The main objectives of the 3D reservoir static model are to predict the reservoir stratigraphic edges and evaluate its hydrocarbon potentiality. Moreover, static model construction aimed at the delineation of geological structure, reservoir management, petrophysical properties distribution, risk reduction and heterogeneity investigation (Merletti and Torres-Verdin, 2010). The areal extent of the reservoir, hydrocarbon thickness (net pay), porosity and saturation provide the volumetric estimate of the in-place hydrocarbon reserves and constitute the key inputs from seismic interpretation, facies and wireline logs to initiate the reservoir static modeling (Niranjan, 2016).

Building a 3D geological model from field and subsurface data is essential to enhance the subsurface geological understanding and provide more vital information and accuracy throughout exploration, development and production cycles. Static model provides the skeleton to capture and combine the seismic structural interpretation and well petrophysical data in a numerically consistent way with known depositional characteristics (Noureldien and Merghany, 2015).

A static reservoir model typically involves three main stages, carried out by experts in the various disciplines (Cosentino, 2001) as follows: structural model, facies model and petrophysical model. The results of these three stages are integrated in a three-dimensional (3D) context, to build an integrated final geological model of the reservoir. This model represents the reference frame for calculating the quantity of original hydrocarbons in-place (OOIP or OGIP), and on the other, forms the basis for the initialization of the dynamic model.

Quality of the static model depends on the quality of facies, wireline logs evaluation and how many input data used for model building. Static model construction aimed at the structural delineation, reservoir management, petrophysical properties distribution, risk reduction and heterogeneity investigation. Three types of models can build the static model according to (Merletti and Torres-Verdin, 2010): Structural model, facies model and petrophysical model.

Structural modeling

The 3D structural model is the process of integrating the geological interfaces such as horizons and faults honoring the fault cuts and throws that have been identified from the well correlation (Mitra and Leslie, 2003). These surfaces should fit the data within an acceptable range, depending on data precision and resolution.

In other means, structural modeling is the reconstruction of the geometrical and structural properties of the reservoir, by defining a map of its structural top and the set of faults running through it. This stage of the work is carried out by integrating interpretations of the geophysical surveys with the available well data.

Steps for Building 3D Structural Model

The 3D structural model is developed according to the following steps (Abdel Gawad et al., 2016; Zhang et al., 2015):

1) Fault modeling
2) Pillar gridding
3) Make horizons
4) Make zones

1) Fault Modeling

Fault modeling is the process of defining faults from seismic interpretation implemented into the geological model by generating fault pillars of network faults connected to each other which are known as key pillars (Du et al., 2015). Key pillars are lines that define the slope, angle and shape of the fault. Along each of these lines there are shape points to adjust the shape of the fault to match the input data. The key pillars are generated based on the input data such as fault sticks and fault polygons. The fault modelling starts with picking the faults on the 2D seismic sections to create the fault sticks. Then, the faults sticks are grouped by Petrel software to construct the fault surfaces. These fault surfaces indicate the dip, azimuth, length and orientation of the interpreted faults.

In the study area, the interpreted fault polygons on the tops of the Middle A/R “G”, Middle A/R “G” Limestone, Lower A/R “G”, Lower A/R “G” Limestone, Upper Bahariya and Lower Bahariya surfaces had been loaded into Petrel software and utilized to build the fault model. Fault sticks (**Fig. 6**) of the major faults were used to guide the 3D fault modelling process. Then, the faults sticks are used to construct the fault surfaces (Fig. 7).

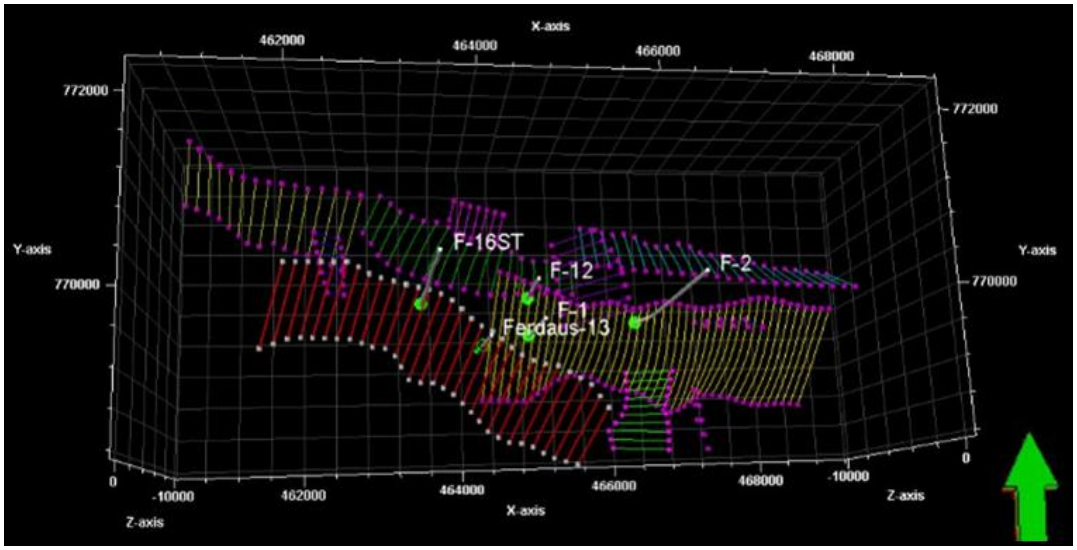

Fig. (6): Fault sticks of Ferdaus oil field in a 3D view.

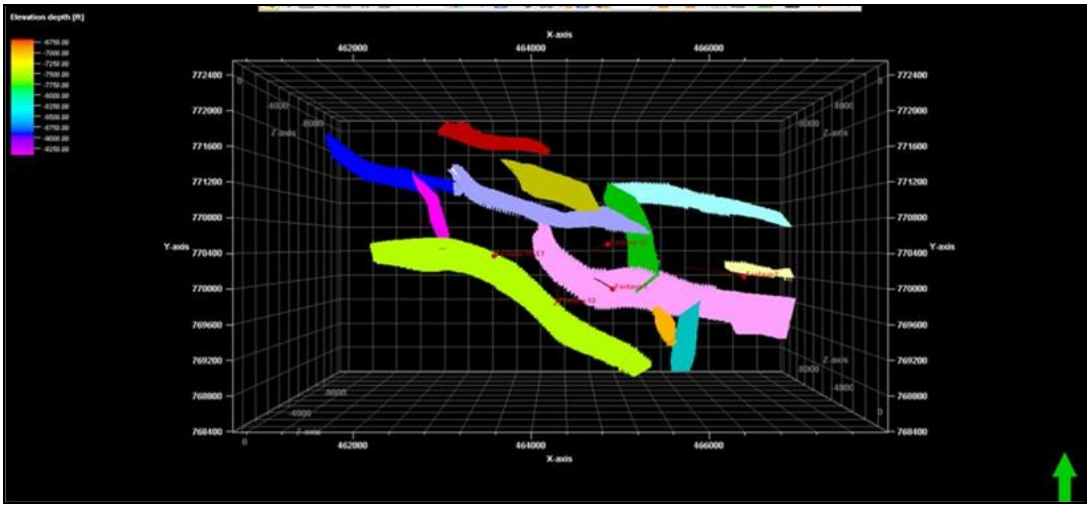

Fig. (7): Fault surfaces of Ferdaus oil field in a 3D view.

2) Pillar Gridding

Pillar gridding is the process of generating spatial framework of the grid skeleton for the 3D model and to limit the model in the I and J directions (Zhang et al., 2015). The skeleton grid is constructed to detect the volume of the model in the space. The grid is represented by pillars (coordinate lines) that define the corners of the 3D cells. Trends and directions are used to guide the gridding process and to control the orientation of the grid cells. The 3D grid consists of top, mid and base skeleton grid each is attached to the top, mid and base points of the key pillars. In addition to the three skeleton grids there are pillars connecting every corner of every grid cell to their corresponding corners on the adjacent skeleton grids.

The resulted fault planes from the fault modeling can be given in two directions, I and J, where the I direction is parallel to faults direction, while the J direction is perpendicular to them. There is also another given direction which is called A (arbitrary direction) this direction is given to the faults that do not follow either I or J direction (Noureldien and Merghany, 2015). The resulted 3D skeleton grid should be edited from any inconsistency in the input data (seismic surfaces, well tops, and dip angle) to get more accurate 3D grid.

The goal of the pillar gridding process is to create distributed rectangular shaped grid cells. The grid used in Ferdaus oilfield is 50 m × 50 m × 1 m (Fig. 8). There are three skeleton grids as a result of the pillar gridding of the Ferdaus oil field model; the top, middle and bottom skeletons. These skeletons are the architecture of the structure model and will be used in building the horizons and zones.

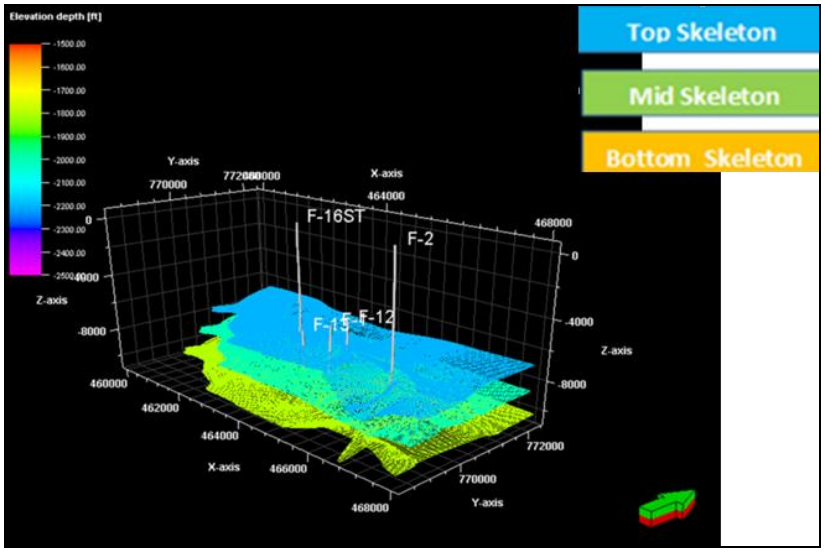

Fig. (8): Pillar skeleton grids at Ferdaus oil field.

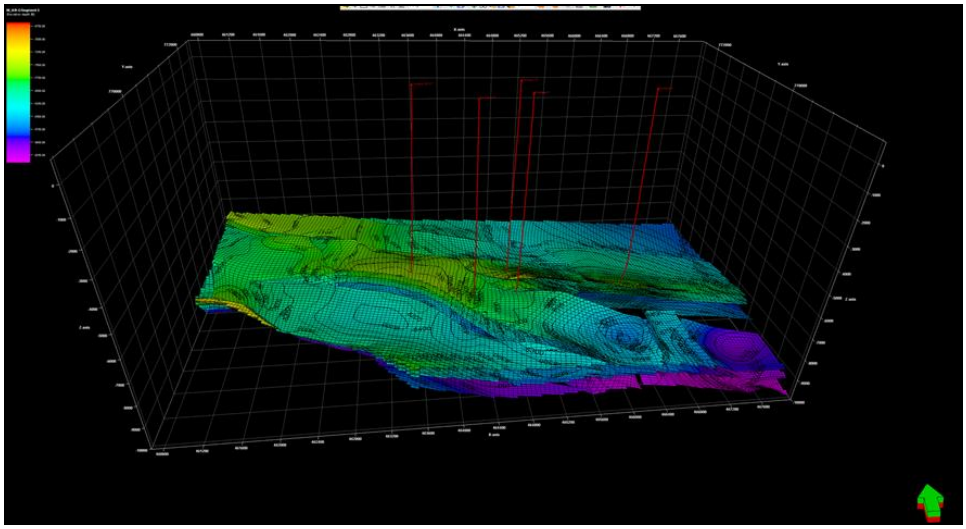

Fig. (9): Horizon model of the Ferdaus oil field.

3) Make Horizons

The make fault framework model and pillar gridding processes are completed, adding horizons is the next step in the workflow. The make horizons is the process of inserting the surfaces of stratigraphic horizons in the model (3D grid) from XYZ input data, while honoring the faults defined in the fault modeling (Zhang et al., 2015). It is considered as a first step in defining the vertical layering of the 3D grid in Petrel software. The 3D grid will have many main layers than the number of seismic surfaces inserted into the three grid skeleton. Fig. (9) represents the horizon model of the five interested seismic horizons: Middle A/R "G", Middle A/R "G" Limestone, Lower A/R "G", Upper Bahariya and Lower Bahariya.

Fault model, pillar gridding, and make horizons processes are always considered together. It is normally checked in go, back, and forth between them. Problems with the fault model are often not obvious before the beginning of pillar gridding, and problems with the pillar grid may not be obvious before building the horizons with make horizons process. Similarly, many problems identified when using make horizons process will require an edit of the pillar gridding options or even the fault model.

It is recommended to build the model simply at the beginning and go right through these three processes before progressively adding more complexity to the fault model. This helps to identify which features cause problems and how best to solve them.

4) Make Zones (Zonation)

The make zone process creates zones above, below or in between the resulting horizons (Zhang et al., 2015). The zone generating process defines the roof and floor for each formation created in the making horizon process. Zones were added to the model by introducing thickness-isochore data created by the isochore points from well tops. Each formation was set to be one zone.

The zones construction process mainly relied on the petrophysical analysis to better estimate the sub-layering system of Middle A/R "G", Middle A/R "G" Limestone, Lower A/R "G", Lower A/R "G" Limestone , Upper Bahariya and Lower Bahariya. Well tops from correlation and isochore maps were used as input data to generate the needed zones in this area.

The model has been divided into six zones (Fig. 10):

- Middle Abu Roash "G" member as two (layers) zones (reservoir and non-reservoir).
- Middle Abu Roash "G" Limestone member as one zones (non-reservoir).
- Lower Abu Roash "G" member as two zones (reservoir and non-reservoir).
- Lower Abu Roash "G" Limestone member as one zones (non-reservoir).
- Upper Bahariya was divided into two zones (reservoir and non-reservoir).
- Lower Bahariya was divided into one zone (non-reservoir).

The confidence of the horizons picking is highly dependent on the quality of the data. The confidence is high where the data quality is good and moderate where the data quality is fair and the horizons are highly faulted. In general, the quality of the seismic data is fair to good over the study area. The resulted depth structure map (Fig. 5) suggests that the Ferdaus oil field can be divided into separate blocks.

Considering the above-mentioned four processes of the fault modeling, pillar gridding, make horizons and make zones were added together to build the final 3D structural model (Fig. 11). The obtained 3D structural model confirms the interpreted structure from the seismic interpretation. It shows the regional tectonic uplift occurred in the study area and a typical tilted fault block indicated by the mapped faults.

The five wells drilled in the Ferdaus oil field has been studied and confirmed the regional setting of this part of the Western Desert by having northwest-southeast structure trend at Middle and Lower Abu Roash "G" and Bahariya Formation target levels as a big horst block which is divided into smaller three-way dip closure tilted fault blocks by different fault trends.

Generally, Ferdaus structure is a northwest-southeast oriented highly faulted tilted block. Most

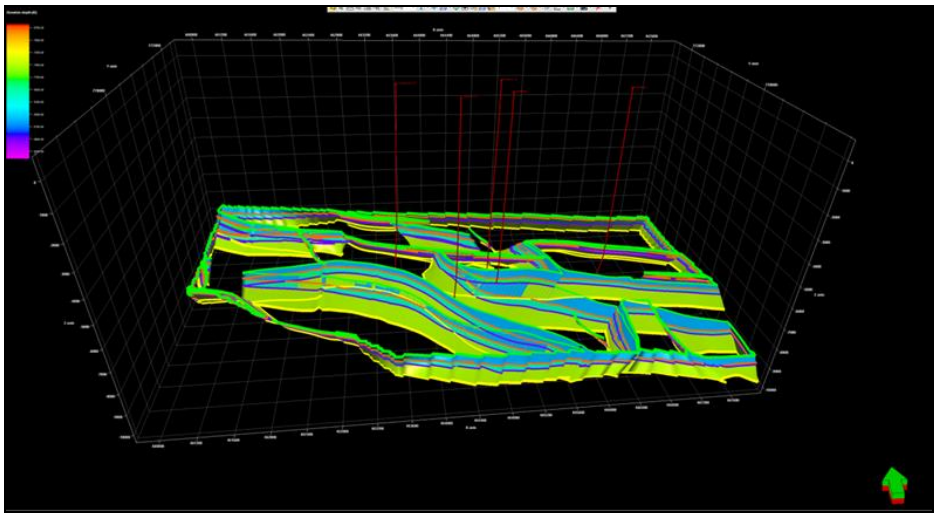

Fig. (10): Zonation model of the Ferdaus oil field in a 3D view.

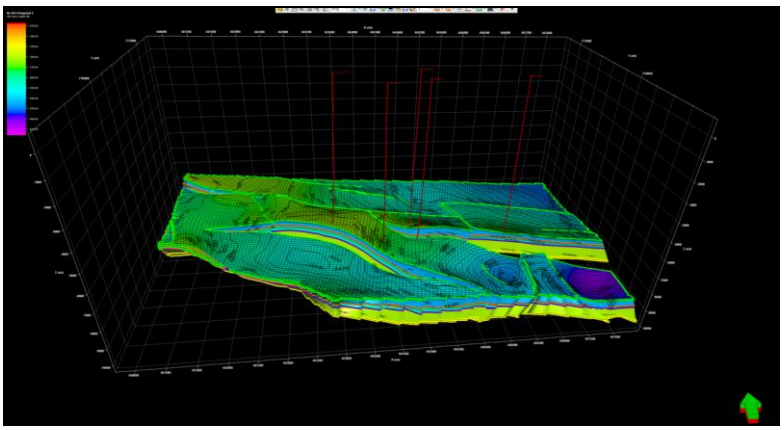

Fig. (11): Final 3D structure model of Ferdaus field.

faults are trending northwest-southeast or east-west, while a few are trending north south.

The structural framework on top of the main reservoirs is provided by three seismically interpreted horizons, namely Middle A/R "G", Lower A/R "G" and Upper Bahariya. The structure on top of the reservoir zones is generated by well tops and isochore maps.

3) Ferdaus Fault Seal Analysis Juxtaposition

Fault seal analysis means the study of the possibility of a fault to allow the fluids to move across the fault plane, whether it is a leak or seal (Yielding et al., 1997). A fault can be a transmitter of/or a barrier to fluid flow and pressure communication. Fault seal can arise from reservoir/non-reservoir (permeable/non-permeable) juxtaposition or by the development of fault rock having high formation pressure. The controlling factors of a fault seal analysis are:

1) The juxtaposition of reservoir against sealing lithology.
2) Deformation during the fault displacement.
3) Subsequent evolution and the current state of stress of the fault/proximity to failure (Yielding et al., 2001). Whilst the stress state of fault relates to the in-situ stress state of fault and the critical stress state, at which a fault may leak (Barton et al., 1995), juxtaposition relates to detailed mapping of an area to identify the reservoir-non reservoir juxtaposition and the possibilities of a non-permeable lithology forming a side seal to reservoirs, across a fault plane. Although in reservoir-reservoir juxtaposition, the possibility of seal still exists, if the fault zones have capillary pressure higher than the reservoirs on either side of it.

A first-order seal analysis involves identifying the reservoir juxtaposition areas over the fault surface, by using the mapped horizons and a refined reservoir stratigraphy defined by isochores at the fault surface.

The second-order phase of the analysis assesses, whether the sand/sand contacts are likely to support a pressure difference. We define two types of lithology dependent attributes: gouge ratio and smear factor. Gouge ratio is an estimate of the proportion of fine grained material entrained into the fault gouge from the wall rocks. Smear factor methods (including clay smear potential and shale smear factor) estimate the profile thickness of shale drawn along the fault zone during faulting. All of these parameters vary over the fault surface, implying that faults cannot simply be designated sealing or non-sealing (Yielding et al., 1997).

A number of **mechanisms** have been recognized whereby the fault planes can act as a seal or leak (Watts, 1987 and Knipe, 1992):

1) **Juxtaposition**, in which reservoir sands are juxtaposed against a low-permeability unit (e.g., shale) with a high entry pressure.
2) **Clay smear** (i.e., entrainment of clay or shale) into the fault plane, thereby giving the fault itself a high entry pressure.
3) **Cataclasis**, which is the crushing of sand grains to produce a fault gouge of finer grained material, again giving the fault a high capillary entry pressure.
4) **Diagenesis**, when preferential cementation along an originally permeable fault plane may partially or completely remove porosity, ultimately creating a hydraulic seal.

There are **several methods** for fault seal analysis utilizing detailed seismic mapping and well analysis.

1. **Allan diagram** to determine the juxtaposed reservoirs (Allan, 1989).
2. **Shale smear factor** to predict the possibility of continuous shale smear on the fault surface (Lindsay et al., 1993).
3. **Pore pressure** distribution and clay smearing, to detect the seal strength of faults (Berg and Avery, 1995).
4. **Shale Gouge Ratio** to predict the sealing capacity of faults (Yielding et al., 1997).
5. **Identify the fluid composition** using geochemical studies of fluid types and pressure (Alexander, 1998).

The most commonly used method in fault seal analysis is the construction of **Allan maps** (Allan, 1989), by using the detailed seismic mapping and well analysis of the different mapped horizons that are defined by isochores at the fault surface.

An important tool for evaluating the flow potential across a fault is a strike view, or map of the fault plane with the hanging wall and footwall intersections superimposed on the modeled fault surface. Allan diagrams use this technique to show the possibility of fluid migration pathways, leak points or sealing areas across the fault. Well tops that identified from correlation of seismic depth maps and well analysis were used as input to generate the needed zones in this area to build the following reservoir and non-reservoir zones.

The zones construction process is mainly relied on the petrophysical analysis to better estimate the reservoir and non-reservoir zones of:

- Abu Roash "F" member as one zone (non-reservoir),
- Upper Abu Roash "G" member as one zone (non-reservoir),
- Middle Abu Roash "G" member as two zones (reservoir and non-reservoir),
- Middle Abu Roash "G" Limestone member as one zone (non-reservoir),
- Lower Abu Roash "G" member as two zones (reservoir and non-reservoir),

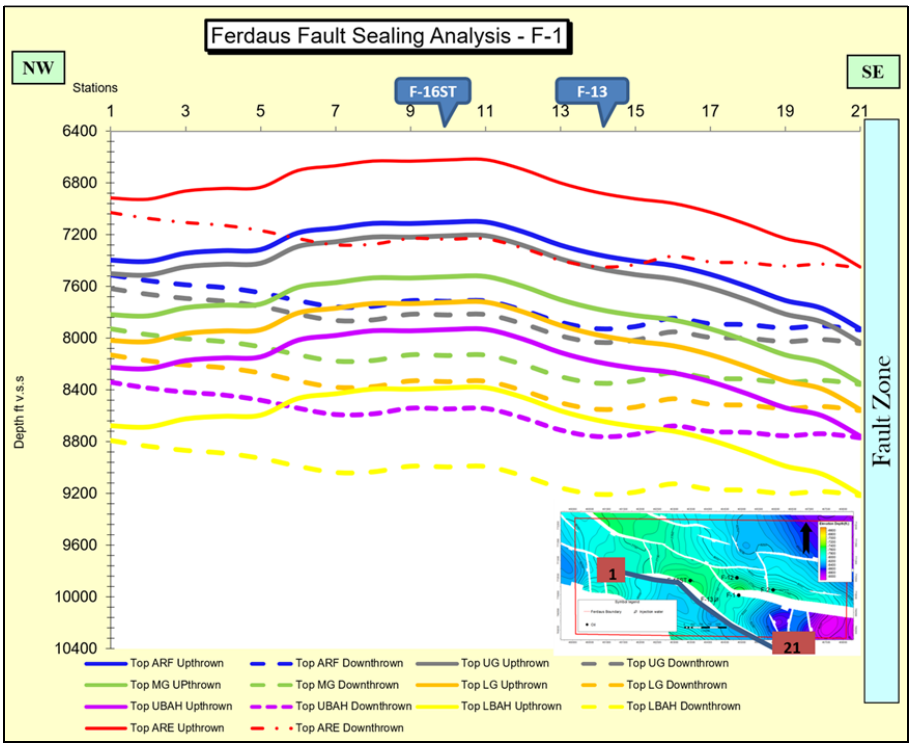

Fig. (12): Allan's diagram of F-1 major normal fault seal analysis at Ferdaus oil field.

- Lower Abu Roash "G" Limestone member as one zone (non-reservoir),
- Upper Bahariya Formation as two zones (reservoir and non-reservoir).

Fig. 12 shows Allan's diagram of the major normal fault trending nearly E-W to NW-SE (F-1). This diagram illustrates the Middle Abu Roash "G" reservoir in the footwall upthrown side juxtaposed by the Upper Abu Roash "G" shale seal Members in the hanging wall downthrown side at stations 1-6, then it is juxtaposed again by a seal silt and shale Abu Roash "E" Member and Abu Roash "F" Limestone at stations 6-17, finally F-1 is juxtaposed at stations 17-21 by Upper Abu Roash "G" shale seal Member.

The Lower Abu Roash "G" reservoir in the footwall upthrown side is juxtaposed by the Middle Abu Roash "G" Sandstone and Limestone seal Member in the hanging wall downthrown side at stations 1-6 and 18-21, then it is juxtaposed again by the Abu Roash "F" Limestone and Upper Abu Roash "G" shale seal Members in the hanging wall downthrown side at stations 6-18.

The Upper Bahariya reservoir in the footwall upthrown side is juxtaposed by the Middle Abu Roash "G" Sandstone and Limestone seal Member and the Lower Abu Roash "G" Sandstone and Limestone seal Member in the hanging wall downthrown side at stations 1-6 and 16-21, the topmost part 200 ft of Upper Bahariya reservoir is juxtaposed by the Upper Abu Roash "G" shale seal Member in the hanging wall downthrown side at stations 6-16.

Conclusions

The five wells drilled in the field tested/identified the regional setting of this part of the Western Desert by having northwest-southeast structure trend at A/R "G" and Bahariya Formation target levels as a big horst block which is divided into smaller three-way dip closure tilted fault blocks by different fault trends. Ferdaus structure is a northwest-southeast oriented highly faulted tilted block. Most faults are trending northwest-southeast or east-west, while a few trend north-south. The structural framework on the tops of the main reservoirs is provided by three seismically interpreted horizons, namely Middle A/R "G", Lower A/R "G" and Upper Bahariya by construction of depth structure maps.

Fault elements were detected from these depth structure maps. F-1 is a major normal fault element trending nearly E-W to NW-SE selected to study the fault seal analysis. Fault seal can arise from reservoir/non-reservoir juxtaposition. Allan diagram method was used to determine the juxtaposed reservoirs for evaluating the flow potential across a fault strike and mapping the fault plane with the hanging wall and footwall intersections superimposed on the modeled fault surface.

The Middle Abu Roash "G", Lower Abu Roash "G" and Upper Bahariya reservoirs in the footwall upthrown are juxtaposed by Abu Roash "E" silt and shale, Abu Roash "F" Limestone and Upper Abu Roash "G" shale seal Members in the hanging wall downthrown side.

Acknowledgement

We deeply acknowledge the Egyptian General Petroleum Corporation for their kindly help and supporting us with the acquired data used in the research.

REFERENCES

Abdel Gawad E.A., Fathy, M., and Attia, M.M., (2016): Subsurface Geological and Petrophysical Analysis Of Bahariya Reservior at Yomna Field, East Bahariya Concession, North Western Desert, Egypt,Vol-2, Issue-6. International Journal of Scientific Engineering and Applied Science (IJSEAS), pp.309-314.

Abdul Azim S., Al-Ajmi, H., Rice C., Bond, D., Abdullah, S., and Laughlin, B., (2003): Reservoir Description and Static Model build in Heterogeneous Mauddud Carbonates Raudhatain Field, North Kuwait. Society of Petroleum Engineers (SPE 81524), Kuwait Oil Company.

Allan, U.S., (1989): Model for Hydrocarbon Migration and Entrapment within Fault Structures, American Association of Petroleum Geologists Bulletin, pp.803- 811.

Alexander, M., (1998): Applications of Geological, Geophysical and Geochemical Data to Investigate 3 Low-pay wells in North Pailin, Pattani Basin, Gulf of Thailand. Msc Thesis, University Brunei Darusalam.

Barton, C.A., Zoback M.D. and Moos, D., (1995): Fluid Flow along Potentially Active Faults in Crystalline Rock, Geology, 23:683-686.

Berg, R.B. and Avery, A.H., (1995): Sealing properties of Tertiary growth faults, Texas Gulf coast. American Association of Petroleum Geologists Bulletin, 79, 375-393.

Cosentino L., (2001): Integrated reservoir studies, Technip, p. 310.

Du, Y., Yang, C., and Peng, Y., (2015): Geomodeling Study in Lithologic Gas Reservoir. In Zhang et al, A Best Practice in Static Modeling of a Coalbed-Methane Field: An Example from the Bowen Basin in Australia. Society of Petroleum Engineers, pp. 151-153.

Knipe, R.J., (1992): Faulting processes and fault seal, in R. M. Larsen, H. Brekke, B. T. Larsen, and E. Talleras, eds., Structural and tectonic modelling and its application to petroleum geology: Amsterdam, Elsevier, p. 325–342.

Lindsay, N.G., Murphy, F.C., Walsh, J.J., Watterson, J., (1993): Outcrop studies of shale smear on fault surfaces: International Association of Sedimentologists Special Publication pp.113–123.

Merletti, G. and Torres-Verdin, C., (2010): Detection and delineation of thin sand sedimentary sequences with joint stochastic inversion of well logs and 3D prestack seismic amplitude data, SPE Reservoir Evaluation and Engineering, No. 13, 246–264.

Mitra, S and Leslie, W., (2003): Three Dimensional Structure Model of the Rhourde el Baguel field, Algeria, AAPG Bull, Vol. 87, pp. 231-250.

Niranjan C. Nanda., (2016): Seismic Data Interpretation and Evaluation for Hydrocarbon Exploration and Production.

Noureldien, D.M and Merghany, I., (2015): Static Model QC: Technical Aspects and Practice from A to Z. Cairo: Society of Petroleum Engineers.

Petrel Software.1.0, (2014): developed by Schlumberger.

Watts, N., (1987): Theoretical aspects of cap-rock and fault seals for single- and two-phase hydrocarbon columns: Marine and Petroleum Geology, v. 4, p. 274–307.

Yielding, G., Freeman, B., Needham, D.T., (1997): Qualitative fault seal prediction,Vol.81,No.6: AAPG Bull. PP.897–917.

Yielding, G., Øverland, J.A, Byberg, G., (2001): Characterization of Fault Zones for Reservoir Modelling: An Example from the Gullfaks Field,North Sea. The American Association of Petroleum Geologists Bulletin.pp.925-951.

Zhang, M., Yang, Y., Xia, Z., Cui, Z., Ren, B., and Zhang, W., (2015): A Best Practice in Static Modeling of a Coalbed-Methane Field: An Example from the Bowen Basin in Australia. Society of Petroleum Engineers, pp. 149-157.

Egyptian Geophysical Society
EGS Journal, Vol. 21, No. 1, 11-19 (2023)

APPLICATION OF GROUND PENETRATING RADAR (GPR) TECHNIQUE TO DETECT POSSIBLE HIDDEN GAPS OR VOIDS IN AN AGRICULTURAL LAND, NAG HAMMADI, QENA, EGYPT

S.B.A. YOUSSEF, M.A. SHAHEEN and M.H.M. YOUSEF

Nuclear Materials Authority, Cairo, Egypt

تطبيق تقنية الرادار للكشف عن الفجوات المخفية المحتملة فى أرض زراعية ، نجع حمادى ، قنا ، مصر

الخلاصة: منطقة الدراسة المختارة هي أرض زراعية تبلغ مساحتها حوالى 600 متر . مربع الهدف الرئيسي من هذه الدراسة هو الكشف عن حجم وعمق الفراغ أو الفجوات الجوفية (المجارى) لمعالجة فقدان مياه الري. تم إجراء ستة عشر ا مقطعا جانبيا باستخدام تقنية الرادار بأطوال مختلفة تتراوح من 32 الى 35 مترا ، مع مسافة فاصلة بني اخلطوط تبلغ 1 متر . يشمل التعامل مع هذه البيانات تفسير خطوط المسح الرادارى للكشف عن مواقع الفراغات والكهوف فى المنطقة المختارة ، وتحديد طرق التعامل مع هذه المواقع لتقليل الفاقد من مياه الري. توضح هذه الدراسة مواقع تباينات الالوان المختلفة والانعكاسات العالية واتساع الاشارات المنعكسة ، مقارنة بالتربة المحيطه ؛ كما أن تشتت الاشارات أعلى من الطبقة الحاوية فى هذه المواقع مما قد يكشف عن الفراغات والكهوف المحتملة فى منطقة الدراسة. تتراوح أعماق الاهداف المحتملة من 7.0متر الى 8.0 متر . تم إجراء تحليل ثلاثى الابعاد لمجموع ملفات تعريف GPR لتأكيد وجود الهدف المخفى المحتمل والاعماق الدقيقة لهذه المواقع. تم عمل أربع شرائح زمنية مختلفة (وقت الإختراق فى اتجاهين) ، كما تم عمل مقطعين فى الاتجاه السينى والصادى لإظهار الهدف المخفي المحتمل . تتوافق النتائج مع العمق الذي تم الحصول عليه من الصورة ثنائية الابعاد.

ABSTRACT: *The selected area is an agricultural land of approximately 600 m square. The main target of this study is to detect the size and depth of the subsurface voids or gaps (sinkholes) to treat the problem of irrigation water loss. Sixteen GPR profiles of different lengths were conducted ranging from 32-35 m, with a separation of 1 m width. The interpretation of GPR profiles reveals the locations of the voids in the selected area, and determine the effective ways to deal with these defects. Results showed locations of different color contrasts and high reflections amplitude of the reflected signals, compared to the surrounding soil; also the higher scattering compare to the bed layer in these locations reveals possible voids in the study area. The depths of the possible targets range from 7.0 m to 8.0 m. 3D analysis was performed for the total GPR profiles to confirm the presence of the possible hidden target and the accurate depths of these objects. Four time-slicing at different (two-way travel time) TWTT were selected together with two X-cut and two Y-cut were done to track the possible hidden target. These results were in agreement with the results obtained from the 2D image. Such information reveal the important of Radar technique in handing the geotechnical problems.*

1. INTRODUCTION

The area of the present study is located in the Nag Hammadi city, Qena governorate (Fig. 1). Where a piece l of an agricultural land of approximately an area of 600 m square was selected. During the irrigating of this agricultural land, water seeps into the ground. The downward movement of water may also transport soils, resulting in fertilizing ground loss and surface depressions called "sinkholes", a GPR survey was conducted to determine these subsurface features and the possible occurrence of voids (sinkholes) responsible for the irrigation water loos. The sedimentary succession in the study area belongs to the Nile valley succession of the late Cretaceous to early Eocene, a dry mud and sandy mud overlying the wet sand layer (Said, 1981). Ground-penetrating radar is selected to help identifying the locations of sinkholes in the selected area to determine then options ways to deal with the loss of the irrigation water.

The effectiveness of a geophysical survey is typically conditioned by the existence of contrast between the measured physical properties among the study area. Therefore, considering changes in physical properties of material due to dissolution, erosion, and/or subsidence involved in the development of sinkholes, geophysical methods are excellent tools for indirect investigation (Hoover 2003). In general, the use of geophysical surveys in the characterization of karst terrains consists of the detection and mapping of the extension of sinkholes as well as information about the depth of the water table, direction of the underground flow, and depth of the karst rocks (Chalikakis et al. 2011).

Despite the countless geophysical investigations carried out on karst terrains worldwide, (mainly for mapping cavities) GPR method has proven to be the most efficient geophysical method for identifying geometric karst features. At the past couple of decades the use of the GPR method has increased and many improvements have been successfully implemented (McMechan et al. 1998; Zisman et al. 2005; Kruse et al. 2006; Rodriguez et al. 2014; Sevil et al. 2017; Hussain et al. 2020).

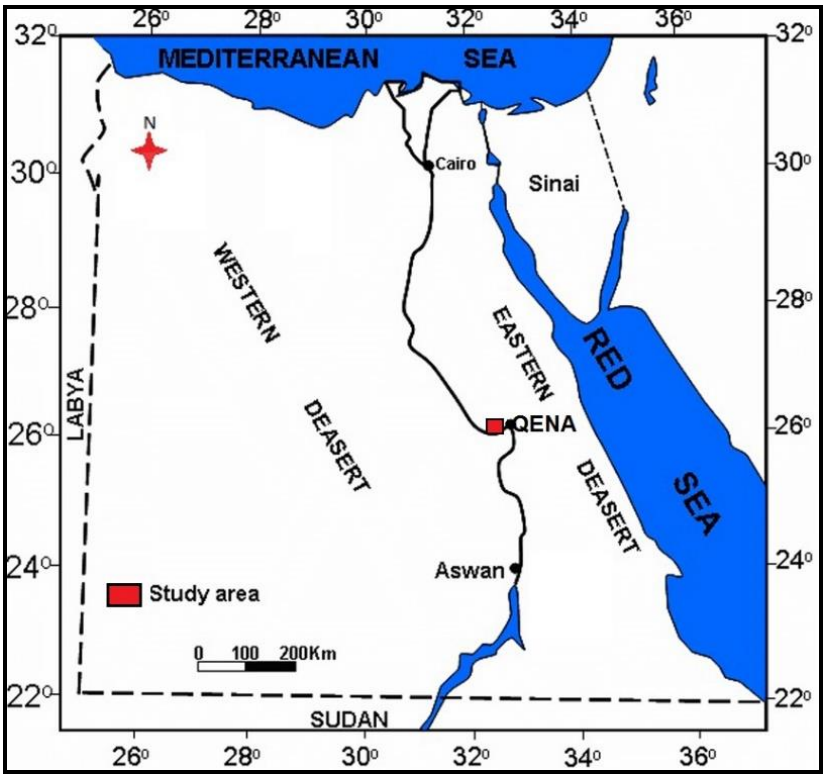

Fig. (1): A location map of the study area.

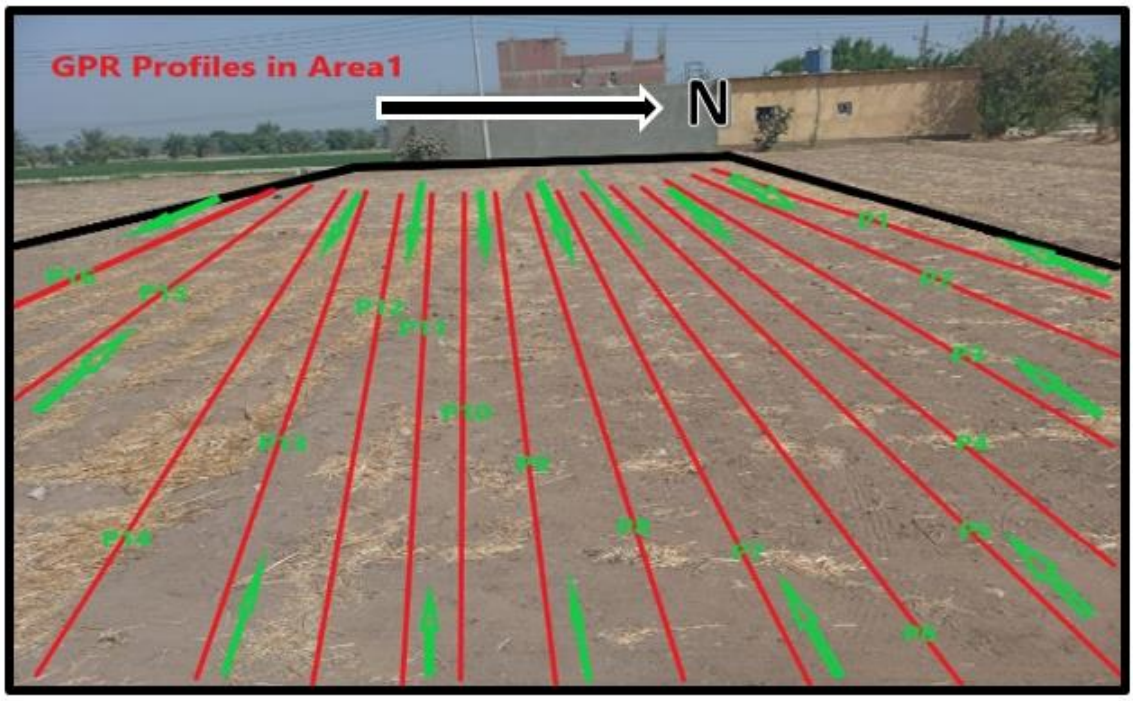

Fig. (2): Location of GPR profiles in the study area.

2. Ground Penetrating Radar (GPR) Survey

2.1. GPR basic concept

The physical principle and data acquisition of GPR methodology are similar to the seismic reflection and the sonar techniques, except for the fact that the GPR is based on the reflection of electromagnetic waves (Casas et al. 2000). According to Annan (2002), this method stands out for shallow investigations, due to its high resolution and the acquisition of a large volume of data in a short period of time. The depth of investigation is a limitation of the GPR method, and is influenced by many factors including geometric scattering, attenuation by the terrain, and partition of energy at the interfaces,

which are all related to the loss of energy during the propagation of the electromagnetic wave (Bradford 2007). The depth of investigation and resolution of GPR vary according to the frequency of the antenna. The higher the frequency, the higher the vertical resolution and the lower the depth of investigation, and vice versa.

A ground-penetrating radar instrument includes a transmitter, a receiver, and a data collection device. The transmitter sends radio pulses from an antenna into the ground. A receiver picks up reflections received from this radio signal, the strength and direction of the reflected signal give the size and depth of the reflecting object (Daniels, 1996). The advantage of GPR is that it records detailed vertical soil profiles rather than just generating horizontal plan maps. It must be remembered that GPR doesn't only image targets in the subsurface, it provides a 2D record of the 3D waves bouncing of objects on the ground (Davis et al., 1989). Linear features which are aligned with the GPR's electrical field will not produce high reflectance values. However, this means that GPR is good at distinguishing linear features if only run perpendicular to the path of the antenna (Sharma, 1997).

2.2. GPR instrument

In the present study, a Sweden MALA GPR system was used with a 100 MHz antennae (Fig. 3). It provides a detailed look at what's beneath the surface. The system offers leading-edge GPR technology, with full digital control to all setup parameters and a multi-channel color display.

2.3. Data collection and processing

Sixteen GPR profiles of E-W direction were conducted of different lengths ranging from 32-35 m, with a line separation of 1 m width.. The objective of this study is to detect the size and depth of subsurface voids (sinkholes) to treat loos of the irrigation water. The conducted GPR data were processed using the software program (Reflex W, 2D/3D). This program is designed for the steps of processing and interpretation of 2D and 3D electromagnetic and seismic reflections. The program supports most formats of the GPR data. As part of the standard filter algorithms, a wide range of special methods is available. The raw GPR data were processed using several parameters and filters to get clear high-resolution 2D GPR profiles (Sato, 2001).

Using ReflexW software, version 7.0 (Sandmeier 2012), the 2D data processing routine comprised:

IMPORT – involve file format conversion (*.dzt - output from SIR3000 equipment, to *.dat format - ReflexW file);

SET TIME ZERO - adjust of the first arrival of the electromagnetic wave;

ENERGY DECAY (gain) - applied to recover the attenuated amplitude of the electromagnetic signal during signal propagation;

BACKGROUND REMOVAL (2D filter) - remove coherent noise related to the reverberation of the electromagnetic wave within the antenna shield and external noises;

BANDPASS (1D filter) – eliminate of electronic and static noise inherent to the system;

LINEAR GAIN – applied to highlight the amplitudes lost with spherical scattering.

2.4. Data interpretation and analysis

GPR is a geophysical tool that produces vertical cross-sectional images of the shallow subsurface, similar to seismic reflection profiles. GPR data

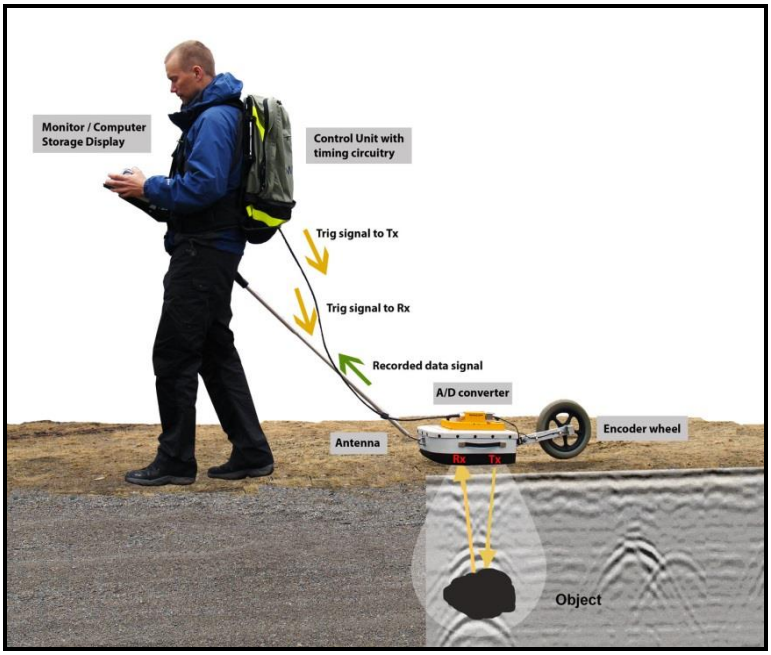

Fig. 3: The used GPR MALA System in the selected area.

collection provides the reflection and scattering of high-frequency electromagnetic waves within the subsurface (Gutierrez et al. 2009 and Mustasaar et al. 2012). If the subsurface layers were homogenous, the GPR instrument could not record any reflections. But earth crust is heterogeneous, and therefore gives radar reflection data to interpret (Hempen and Hatheway, 1992 and Daniels, 1996). The analysis of the reflected GPR signals is important because it gives notice of subsurface changes in lithology and other physical properties. The higher the contrast at a buried object, the greater the amplitude of the reflected waves. The amplitude changes can be related to the presence of important buried objects. The location of high and low reflectivity at specific depths can detect the possible buried objects with the surrounding soil. Areas of low amplitude reflections indicate uniform matrix materials or background soil, while those of high amplitude waves denote areas of high subsurface contrast, such as voids or gap features (Conyers and Goodman 1997). The gathered sixteen GPR profiles were divided into four groups to be processed and analyzed as follows:

A- Group 1 (P_1-P_4)

The length of each of these profiles is 34 m with a separation of one meter (Fig. 4). Observing the reflecting signals of the subsurface media provides information about the hidden layers of underground in these profiles.

In P_1 and P_2, the reflected signals are nearly similar, indicating the lock of possible hidden targets. The arrows in P_2 refer to the locations of possible slop cracks including wet soil, which gives high contrast color for the reflected signals. In P_3 and P_4, the black circles show signals scattering with a different contrast color than the surrounded soil, this indicates the possible gaps or voids as a collection of underground water coming through the slop cracks. The depths of the possible hidden voids are estimated to be about 7 and 8 m for P_2 and P_4 respectively.

B- Group 2 (P_5-P_8)

These profiles have different lengths that range between from 32and34 m with a separation of 1m (Fig. 5). The four GPR profiles include signals reflection, low, medium, and high reflection with a variation in the color contrast. The low and medium reflections refer to the soil bed layers and the high reflection indicates the possible hidden voids. The black arrows show possible slop cracks for passing underground water to possible subsurface voids indicated by the black circles. By visual inspection of the reflected signals inside these circles, reflections and scattering inside the circles are relatively higher than the surrounded soil, so the circles may indicate the presence of possible voids at these locations. The high contrast color of the reflected signals in these profiles may indicat to the wet parts of the soil. The possible hidden gaps or voids have depths of about 7m in P_5 and P_7 profiles and 8m in P_6 and P_8profiles.

C- Group 3 (P_9-P_{12})

This group includes four profiles P_9, P_{10}, P_{11}, and P_{12} (Fig. 6), with various lengths that range from 32to34 m with separation of one meters. Observing the reflected signals compare to the background reflections, there is no marked variation in the strength of these reflections and all are relatively similar in the color contrast except for some locations that have high pink colors. These locations indicate the wet soil and water-saturated parts of the subsurface soil, P_9 and P_{11}profiles. For these reasons, there are no clear voids in profiles, P_{10} and P_{12}.

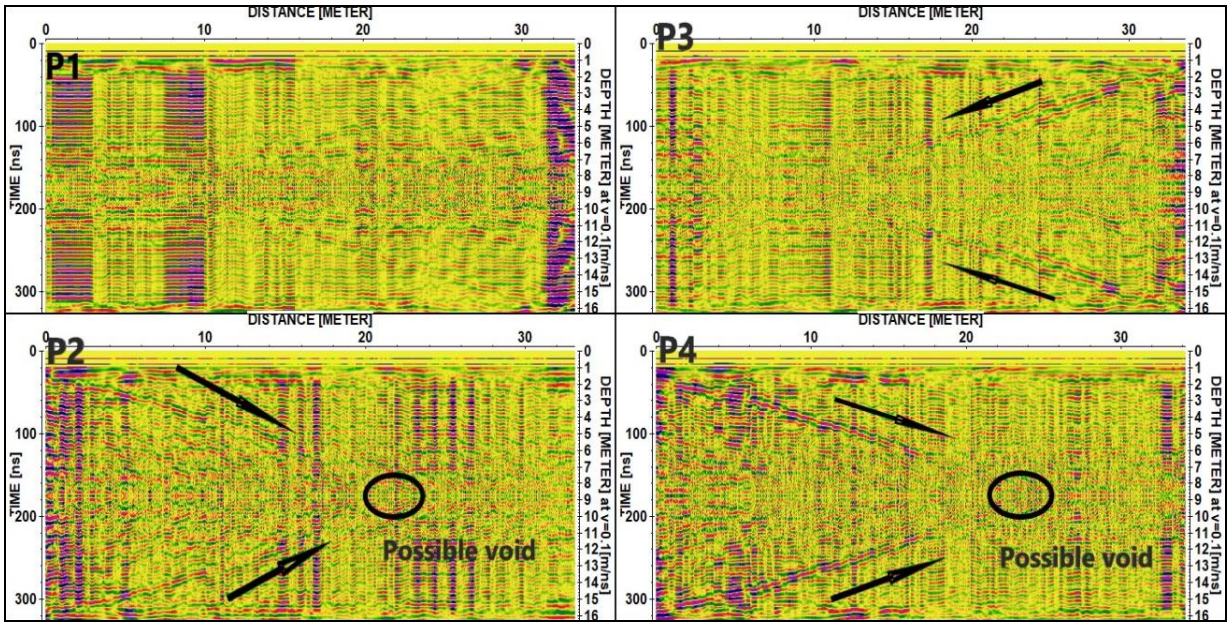

Fig. (4): GPR profiles P_1-P_4.

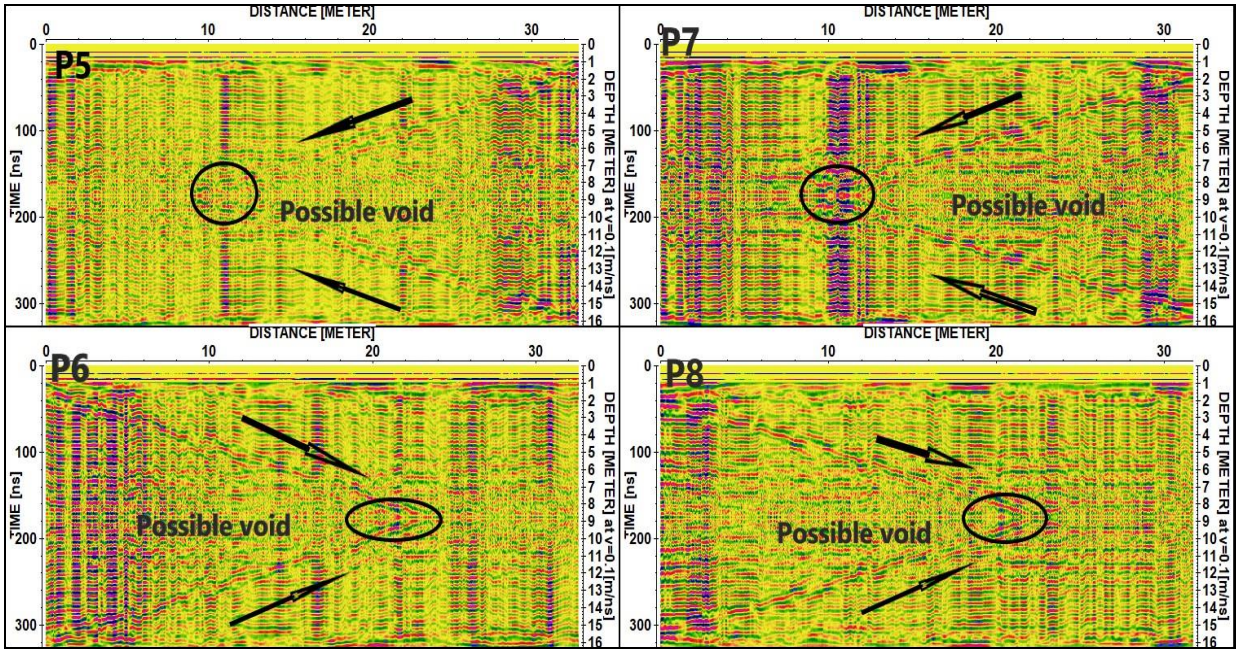

Fig. (5): GPR profiles P_5-P_8.

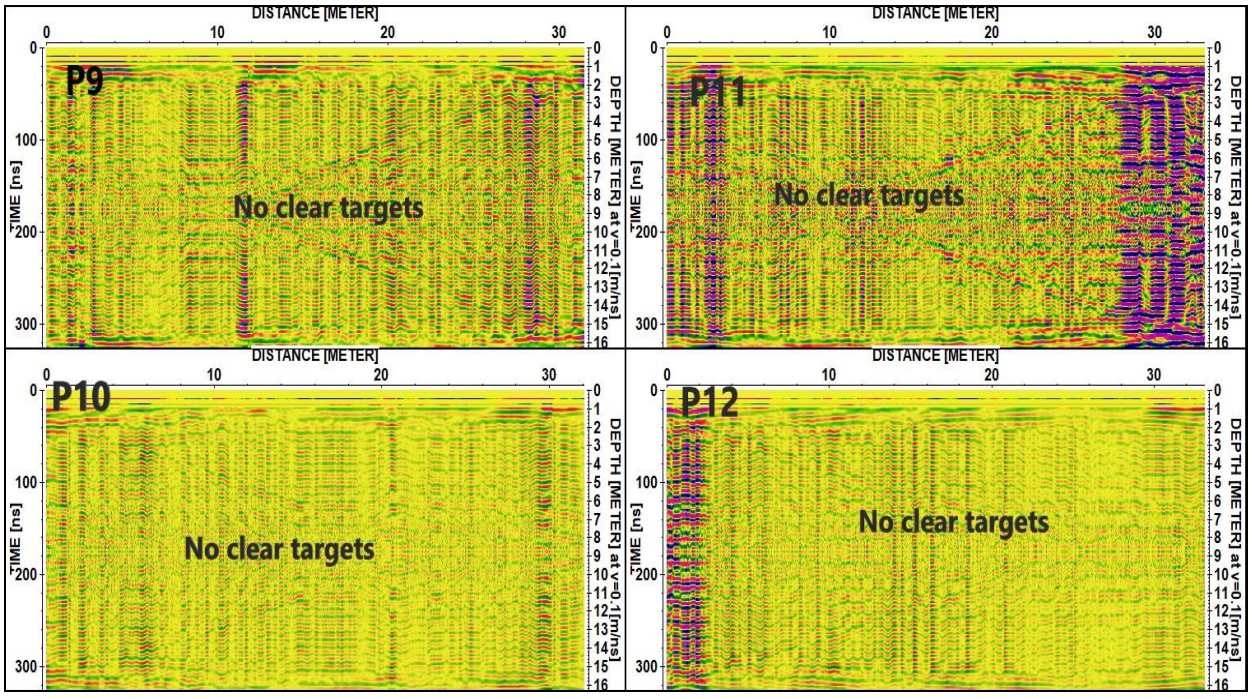

Fig. (6): GPR profiles P_9-P_{12}.

D- Group 4 (P_{13}-P_{16})

The length of the GPR profiles in this group is nearly similar (34m) with a separation of 1m (Fig. 7). Three Profiles (P_{13}, P_{14}, and P_{15}) have no high variation in reflection strength and the signals scattering, so the presence of any hidden voids observed and appear smooth, except for some parts of the soil with high contrast color indicating the wet and water-saturated parts Thus there are no clear evidence of possible hidden targets under these profiles. In the GPR profile (P_{16}), there is a relatively high reflection and scattering (indicated to by the black arrows and circle) for the signals with high contrast color compared to the surrounding soil. These features may indicate the locations of the possible slop cracks and void in this profile. The depth of the possible hidden void is about 7m.

3D Analysis

The GPR data were processed by different filters to improve the quality of the profiles for a perfect interpretation of the 2D radar images and delineating the depths of the hidden features. The results of the GPR data interpretation showed that the depths of these targets are 7m in profiles (P_2, P_5, P_7, and P_{16}) and were 8m in profiles (P_4, P_6, and P_{80}), equivalent to the TWTT of (140 - 190 ns). 3D analysis was performed on total GPR profiles to confirm the presence of the possible hidden features and estimates accurate depths of these objects. Four time-slicing at different TWTT were made (Fig. 8), two X-cut (10, 14 m. distance) and two Y-cut were performed at distances of 6 and 10 m (Fig. 9).

The time slices, X-cut and Y-cut confirm the presence of possible hidden target at TWTT ranges from 140 ns to 190 ns. These results are in agreement with the depth estimated from the 2D images, but the 3-D data analysis for the GPR data enabled better realization to the hidden features. The total information of the possible hidden voids (sinkholes) are gathered for presentation in Table 1.

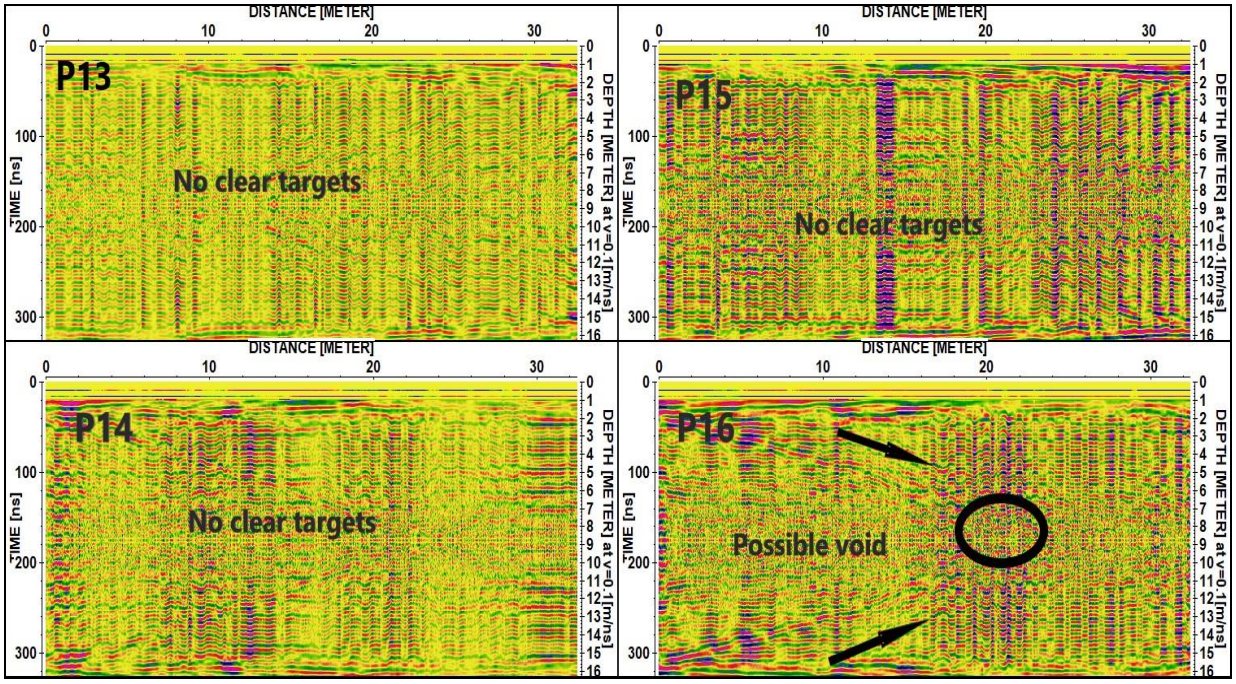

Fig. (7): GPR profiles P_{13}-P_{16}.

Table (1): The total information of the hidden possible voids (sinkholes) in the conducted GPR profiles of the study area.

Profile No.	Approximately TWTT	Approximately Depth	Approximately Size	shape
P2	140-190 ns	7m	2.5m	oval
P4	140-185 ns	8m	3m	oval
P5	140-180 ns	7m	3m	circular
P6	140-190 ns	7m	4m	oval
P7	140-180 ns	8m	3m	circular
P8	140-190 ns	8m	3.5m	oval
P16	140-190ns	7m	3m	Nearly circular

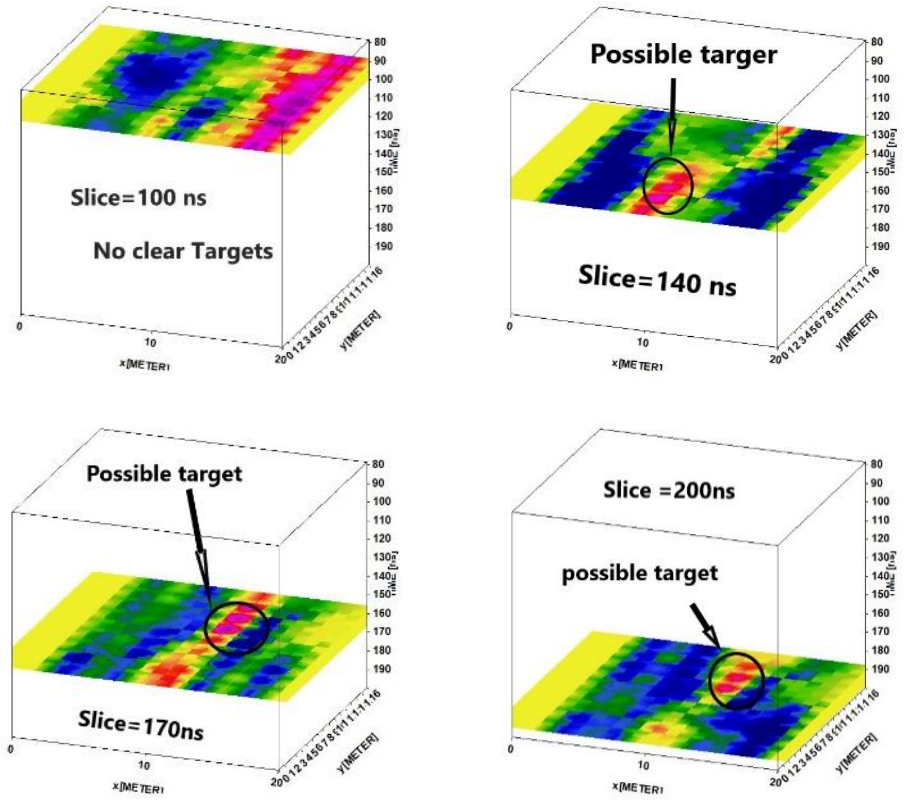

Fig. (8): 3D time slicing for the total GPR profiles.

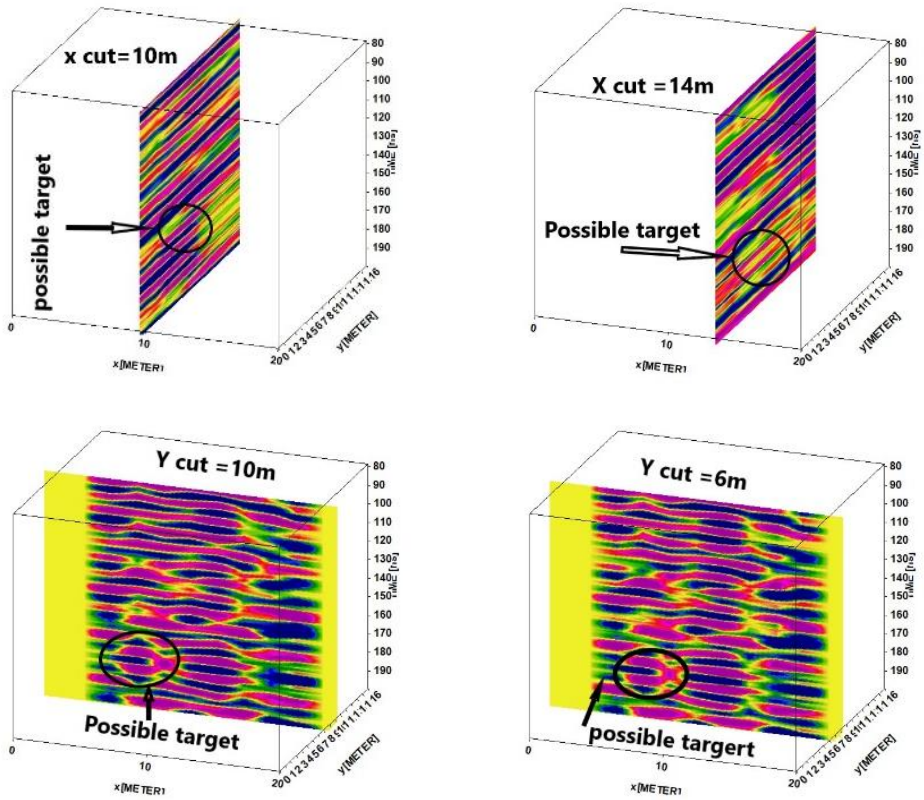

Fig. (9): 3D X-cut and Y-cut for the total GPR profiles.

CONCLUSIONS

The aim of the present study is to detect the subsurface voids or gaps (sinkholes) in the selected area to make up the loss of the irrigation water using the GPR technique. For this purpose, 16 GPR profiles were conducted of different lengths ranging from 32-35 m, with a line separation of 1 m. using the antenna of 100 MHz. The obtained GPR profiles were processed using the software program (Reflex W, 2D/3D) using different filters for achieving sound interpretation. The sixteen GPR profiles were divided into four groups, each one including four profiles.

The interpretation of GPR profiles from P_1 to P_{16}, reveals the locations of some possible voids or gaps (sinkholes), depending on the strength of wave reflections with its color contrast and amplitudes relative to the surrounding soil. These locations show different contrasts and high amplitudes of the reflected signals, compared to the surrounding soil. The scattering of the signals may be higher than the surrounded bed layers in these locations, which may reveal the presence of the possible voids or gaps in the study area.

The GPR data were processed in different ways to filter the profiles from noises to be interpreted accurately for the 2D radar images and to delineate the depths of the hidden possible targets. The results of the GPR data interpretation indicated that the depths of these targets were at 7m in profiles (P_2, P_5, P_7, and P_{16}) and at 8m in profiles (P_4, P_6, and P_8) which are equal to the TWTT of (140-190 ns). 3D analysis was performed for the total GPR profiles to confirm the presence of the possible hidden target and the accurate depths of these objects. Four time-slicing at different TWTT were made, also two X-cut at 10 and 14 m distance, and two Y-cut were done at distance 6 and10 m. The time slices, X-cut and Y-cut show the possible hidden target at TWTT ranges from (140- 190 ns). These results are in agreement with the depth obtained from the 2D image.

REFERENCES

Annan, A.P., 2002: GPR – History, Trends, and Future Developments. Subsurface Sensing Technologies and Applications. Vol. 3 (4): 253-270. https://doi.org/10.1023/A:1020657129590.

Bradford, J.H., 2007: Frequency-dependent attenuation analysis of ground-penetrating radar data. GEOPHYSICS, 72(3), J7–J16. https://doi:10.1190/1.2710183

Casas, A., Pinto, V., Rivero, L., 2000: Fundamental of ground penetrating radar in environmental and engineering applications. Ann. Geophys. 43 (6).

https://doi.org/10.4401/ag-3689

Chalikakis, K., Plagnes, V., Guerin, R., Valois, R., & Bosch, F.P., 2011: Contribution of geophysical methods to karst-system exploration: an overview. Hydrogeology Journal, 19(6), 1169–1180.

https://doi:10.1007/s10040-011-0746-x.

Conyers, Lawrence B. and Dean Goodman, 1997: Ground-penetrating Radar: An Introduction for Archaeologists. Alta Mira Press, Walnut Creek, California.

Daniels, D.J., 1996: Surface-penetrating radar, in, IEEF Radar, Sonar, Navigation and Avionics Series 6, E. D. R.

Davis, J.L., and Annan, A.P., 1989: Ground-penetrating radar for high-resolution mapping of soil and rock stratigraphy. Geophysical prospecting, v.3e7, P. 531-551.

Gutierrez, J.P., Galve, P., Lucha, J., Bonachea, L., Jorda, R., 2009: Investigation of a large collapse sinkhole affecting a multi-storey building by means of geophysics and the trenching technique (Zaragoza city, NE Spain) Environ Geol 58:1107–1122.

Hempen, G.l., and A.W., Hatheway, 1992: Geophysical methods for hazardous waste site characterization, special pub. No. 3: Assn. Eng. Geol.

Hoover, R.A., 2003: Geophysical Choices for Karst Investigations. Sinkholes and the Engineering Environmental Impacts of Karst. https://doi.org/10.1061/40698 (2003)48.

Hussain, Y., Uagoda, R., Borges, W.R., Nunes, J., Hamza, O., Condori, C., Aslam, K., Dou, J., Cárdenas-Soto, M., 2020: The potential use of methods to identify cavities, sinkholes and pathways for water infiltration: a case study from Mambaí, Brazil. Online in https://doi.org/10.1002/essoar.10503456.1

Kruse, S., Grasmueck, M., Weiss, M., Viggiano, D., 2006: Sinkhole structure imaging in covered Karst terrain. Geophysical Research Letters, 33(16).

https://doi:10.1029/2006gl026975 .

McMechan, G.A., Loucks, R.G., Zeng, X., Mescher, P., 1998: Ground penetrating radar imaging of a collapsed paleocave system in the Ellenburger dolomite, central Texas. Journal of Applied Geophysics, 39(1), 1–10.

https://doi:10.1016/s0926-9851 (98)00004-4

Motoyuki Sato, 2001: Jung-Ho Kim, RADPRO/GPR V.3.0 User's Guide.

Mustasaar, M., Plado, J. & Jõeleht, A., 2012: Determination of electromagnetic wave velocity in horizontally layered sedimentary target: a ground penetrating radar study from Silurian limestone, Estonia. Acta Geophysica, 60, 357–370

Rodriguez, V., Gutiérrez, F., Green, A.G., Carbonel, D., Horstmeyer, H., Schmelzbach, C., 2014: Characterizing Sagging and Collapse Sinkholes in a Mantled Karst by Means of Ground Penetrating Radar (GPR). Environmental & Engineering Geoscience, 20(2), 109–132.

https://doi:10.2113/gseegeosci.20.2.109.

Said, R., 1981: The geological evolution of the River Nile. Springer-Verlag, NewYork, 151P.

Sandmeier, K.J., 2012: REFLEXW Version 7.0 for Windows 9x/2000/NT/XP. Program for the processing of seismic, acoustic or electromagnetic reflection, refraction and transmission data. Manual do Software, 192p

Sevil, J., Gutiérrez, F., Zarroca, M., Desir, G., Carbonel, D., Guerrero, J., Linares, R., Roque, C., Fabregat, I. 2017: Sinkhole investigation in an urban area by trenching in combination with GPR, ERT and high precision leveling. Mantled evaporite karst of Zaragoza city, NE Spain. Engineering Geology, 231, 9–20.

https://doi:10.1016/j.enggeo.2017.10.009

Sharma, Prem V., 1997: Environmental and Engineering Geophysics. Cambridge university press. United Kingdam.

Zisman, E.D., Wightman, M.J., Taylor, C., 2005: The Effectiveness of GPR in Sinkhole Investigations. Sinkholes and the Engineering and Environmental Impacts of Karst. https://doi:10.1061/40796 (177) 65.